Published in final edited form as:
J Appl Phys. 2006 March 29; 99(6): 066112. doi:10.1063/1.2186371.

A Phantom Study of Magnetoacoustic Tomography with Magnetic Induction (MAT-MI) for Imaging Electrical Impedance of Biological Tissue

Xu Li, **Yuan Xu**, and **Bin He***
Department of Biomedical Engineering University of Minnesota

Abstract

An experimental feasibility study was conducted on Magnetoacoustic-Tomography with Magnetic Induction (MAT-MI). It is demonstrated that the 2-dimensional (2D) MAT-MI system can detect and image the boundaries between regions of different electrical conductivity with high spatial resolution. Utilizing a magnetic stimulation coil, MAT-MI evokes magnetically induced eddy current in an object which is placed in a static magnetic field. Because of the existence of Lorenz forces, the eddy current in turn causes acoustic vibrations, which are measured around the object in order to reconstruct the electrical impedance distribution of the object. The present experimental results from the saline and gel phantoms are promising and suggest the merits of MAT-MI in imaging electrical impedance of biological tissue with high spatial resolution.

Magnetoacoustic Tomography with Magnetic Induction (MAT-MI) is an imaging modality combining pulsed magnetic stimulation with sonography and it is proposed for imaging the electrical impedance of samples noninvasively[1]. Noninvasive measurement of electrical properties of biological tissue has drawn substantial research interest for decades and a variety of techniques has been developed such as Electrical impedance tomography (EIT) [2–4], Magnetic Resonance Electrical Impedance Tomography (MREIT) [5–7], and Magnetic Induction Tomography (MIT) [8, 9]. In addition, Magnetoacoustic Tomography (MAT) [10, 11] and Hall Effect Imaging (HEI) [12, 13] have both been reported for combining bioelectromagnetism together with sonography.

In the MAT-MI approach we investigated here, pulsed magnetic stimulation (μs) is imposed on an object placed in a static magnetic field. The magnetically induced eddy current is then subject to Lorenz force. The Lorenz force causes acoustic vibrations which can be measured to reconstruct the conductivity distribution of the sample. Denoting the static magnetic field as $\mathbf{B}_0$, the magnetically induced current density distribution as $\tilde{\mathbf{J}}$ (the tilt over a variable indicates a function of time; otherwise, the variable is not a function of time if not denoted explicitly), the Lorenz force can be described as $\tilde{\mathbf{J}} \times \mathbf{B}_0$. The wave equation governing the pressure distribution $\tilde{p}$ can be written in equation (1)[11]

$$\nabla^2 \tilde{p} - \frac{1}{c_s^2} \frac{\partial^2 \tilde{p}}{\partial t^2} = \nabla \cdot (\tilde{\mathbf{J}} \times \mathbf{B}_0) \tag{1}$$

*Correspondence: Bin He, Ph.D., University of Minnesota, Department of Biomedical Engineering, 7-105 Hasselmo Hall, 312 Church Street SE, Minneapolis, MN 55455, e-mail: binhe@umn.edu.

where c_s is the acoustic speed in the media. In equation (1), $\tilde{\mathbf{J}}(\mathbf{r}, t) = \mathbf{J}(\mathbf{r})\delta(t)$, with an assumption that the induced eddy current has an ideal pulsed distribution over time. This would be a reasonable approximation as long as the excitation coil is sending pulse stimulations that are short enough. Using Green's function, the solution of equation (1) can be written as in (2):

$$\tilde{p}(\mathbf{r},t) = -\frac{1}{4\pi}\int_V d\mathbf{r}' \nabla_{\mathbf{r}'} \cdot [\mathbf{J}(\mathbf{r}') \times \mathbf{B}_0(\mathbf{r}')]\frac{\delta(t - R/c_s)}{R} \tag{2}$$

where $R = |\mathbf{r} - \mathbf{r}'|$, and V is the volume containing the acoustic source. The pressure on a surface surrounding the object can be measured to reconstruct the source term $\nabla \cdot (\mathbf{J} \times \mathbf{B}_0)$ using the time reversing technique [1, 14] as in equation (3):

$$\nabla \cdot (\mathbf{J} \times \mathbf{B}_0) \approx \frac{1}{2\pi c_s^2}\int\int_\Sigma dS_d \frac{\mathbf{n}\cdot(\mathbf{r}_d - \mathbf{r})}{|\mathbf{r} - \mathbf{r}_d|^2}\tilde{p}''(\mathbf{r}_d, |\mathbf{r} - \mathbf{r}_d|/c_s)/c_s \tag{3}$$

where $\mathbf{r}_d$ is a point on the detection surface Σ, $\mathbf{n}$ is the normal vector of Σ at $\mathbf{r}_d$, $\mathbf{r}$ is a point in the object, the double prime refers to the second derivative over time. In deriving equation (3) an item of $\tilde{p}'$ is ignored because it is much smaller than the $\tilde{p}''$ item in high frequency as around MHz range.

According to Faraday's law and Ohm's law, we have

$$(\nabla \times \mathbf{J})/\sigma + \nabla(\frac{1}{\sigma}) \times \mathbf{J} = -\mathbf{B}_1 \tag{4}$$

where $\mathbf{B}_1$ refers to the space function of the pulsed magnetic field, which has a step function distribution over time according to Faraday's Law [1]. For a piecewise homogeneous medium [15], the conductivity (other than the boundary points) can be calculated as in equation (5) [1],

$$\sigma \approx -\frac{(\nabla \times \mathbf{J}) \cdot \mathbf{B}_0}{\mathbf{B}_1 \cdot \mathbf{B}_0} \tag{5}$$

where $(\nabla \times \mathbf{J}) \cdot \mathbf{B}_0 = \nabla \cdot (\mathbf{J} \times \mathbf{B}_0)$, because of $\nabla \times \mathbf{B}_0 = 0$.

MAT-MI uses pulsed magnetic stimulation and induces a pulsed solenoid electrical field in the object. This induced electrical field can cause high frequency ultrasound waves which enable the MAT-MI approach to obtain a high spatial resolution impedance image. The present phantom study is aimed at demonstrating the feasibility of the MAT-MI approach in imaging physiological saline solutions simulating biological tissue.

The diagram of our current experiment setup for MAT-MI is shown in Fig. 1. The magnetic stimulator can send pulsed stimulation (μs) through the coil above the sample. The ultrasound sensor driven by the step motor can scan around the sample in a circular orbit. Data acquisition is synchronized with the magnetic stimulation. This composes a 2-D MAT-MI system. Because the reconstruction algorithm shown in (3) and (4) are intrinsic 3-dimensional (3D) and require acoustic measurement on a surface surrounding the sample to quantitatively reconstruct the

conductivity distribution, this 2-D system provides an simplified means of collecting the acoustic signals. However, it's demonstrated that this 2-D system can still reconstruct the conductivity boundaries of the sample in the scanning cross section. The reconstruction algorithm thus can be simplified to (6)

$$I(\mathbf{r}) = -\sum_{i=1}^{N} \frac{\mathbf{r}_i \cdot (\mathbf{r}_i - \mathbf{r})}{|\mathbf{r} - \mathbf{r}_i|^2} \tilde{p}\,(\mathbf{r}_i, |\mathbf{r} - \mathbf{r}_i|/c_s) \tag{6}$$

where $\mathbf{r}_i$ is the position of the sensor at the *i-th* scanning point, $\tilde{p}$ is the pressure signal after removal of low frequency disturbance by filtering.

In the experiment setup, the pulse width of the stimulation is 0.5 μs. The radius of the coil is 40mm. A permanent magnet (50 mm by 50 mm by 25 mm) is placed 2 cm under the sample and creates a magnetic field about 0.1 T along the z-axis at 2 cm from its surface. The transducer (TC3029, Reson Inc.) has a central frequency of 500 KHz. The transducer signal is amplified by 80 dB and sampled at 5 MHz. Because of the limited signal-to-noise ratio (SNR), 100,000 times of averaging at the rate of 500 Hz were used.

Reconstructed images of saline samples with different salinities are shown in Fig. 2. The image center is the origin of the scanning circle orbit. The saline samples are put in a plastic cup and emerged in water. This creates a conductivity step which is analog to a homogeneous tissue with higher conductivity embedded in a low conductive one. The transducer scans the sample with a 2.5 degrees step. The right bottom image in Fig. 2 (water sample) indicates that the plastic cup has little influence on the reconstructed image. It is shown that the current system can distinguish the conductivity difference between water and saline sample with salinity of 1%. In addition, it is obvious that the image boundary intensity positively correlated with the salinity thus the conductivity contrast of the sample and background.

Fig. 3 shows the reconstructed images of double layer gel phantoms with different inner layer size and shape. The salinity is 10% for the outer layer and 0% for the inner layer. Plastic film was inserted between the inner layer and outer layer gel to prevent diffusion. The transducer's scanning step is 2.5 degrees. It is shown in Fig. 3 that the shape and size of the conductivity boundaries in the obtained images are consistent with the real sample.

Fig. 4 shows another example of the MAT-MI image of a gel phantom. Two columns of gels (a cylinder shape and a square prism shape) with 0% salinity are embedded in gel of 10% salinity with plastic film inserted. The scanning step is 1.25 degree. As seen in Fig. 4, the 2-D MAT-MI image is consistent with the cross section of the phantom in terms of shape and size of the conductivity boundary. In addition, more scanning steps in this case led to a better quality image with less backprojection artifacts.

From the current results, it is shown that the width of all the conductivity boundaries in the reconstructed image extends to about 3mm, indicating an "effective" spatial resolution of 3mm. Here we define the spatial resolution as the diameter of the smallest structure that can be reconstructed using the current 2-D MAT-MI setup. This is partly demonstrated in Fig. 4 that the shortest distance between the inner square prism boundary and the outer layer boundary is 4mm, which is clearly seen in the reconstructed image. Higher spatial resolution may be obtained by increasing the transducer central frequency and measurement SNR.

The present experiment results from imaging the saline and gel phantoms, which have close conductivity values to those of biological tissue, are promising, demonstrating the feasibility

and performance of MAT-MI approach to image electrical impedance of biological tissue with high spatial resolution. Further investigation on 3-D MAT-MI system with high signal-to-noise ratio may lead to the establishment of an important noninvasive method for electrical impedance imaging.

In summary, we have demonstrated the MAT-MI approach through a phantom experiment study using the current 2-D system. Conductivity boundary images with high spatial resolution have been obtained from saline and gel phantom indicating the feasibility of MAT-MI and its merits for further investigation.

Acknowledgements

This work was supported in part by NIH RO1EB00178, NSF-BES-0411898, NSF-BES-0411480 (B.H.), and the Biomedical Engineering Institute of the University of Minnesota.

References

1. Xu Y, He B. Physics in Medicine and Biology 2005;50:5175. [PubMed: 16237248]
2. Paulson K, Lionheart W, Pidcock M. IEEE Trans Med Imag 1993;12:681.
3. Metheral P, Barber DC, Smallwood RH, Brown BH. Nature 1996;380:509. [PubMed: 8606768]
4. Mueller JL, Isaacson D, Newell JC. IEEE Trans Biomed Eng 1999;46:1379. [PubMed: 10582423]
5. Joy M, Scott G, Henkelman M. Magnetic Resonance Imaging 1989;7(1):89. [PubMed: 2918822]
6. Kwon O, Woo E, Yoon J, Seo JK. IEEE Trans Biomed Eng 2002;49:160. [PubMed: 12066883]
7. Gao N, Zhu S, He B. Physics in Medicine and Biology 2005;50:2675. [PubMed: 15901962]
8. Peyton AJ, Yu ZZ, Lyon G, Al-Zeibak S, Ferreira J, Velez J, Linhares F, Borges AR, Xiong HL, Saunders NH, Beck MS. Measurement Science and Technology 1996;7:261.
9. Griffiths H. Measurement science and technology 2001;12:1126.
10. Towe BC, Islam MR. IEEE Trans BiomedEng 1988;35:892.
11. Roth BJ, Basser PJ, Wikswo JP Jr. IEEE Trans BiomedEng 1994;41:723.
12. Wen H, Shah J, Balaban S. IEEE Trans BiomedEng 1998;45:119.
13. Wen H. Ultrasonic Imaging 2000;22:123. [PubMed: 11061463]
14. Xu Y, Wang LHV. Phys Rev Lett 2004;92:033902. [PubMed: 14753876]
15. He, B., editor. Modeling and Imaging of Bioelectrical Activity – Principles and Applications. Kluwer Academic Publishers; 2004.

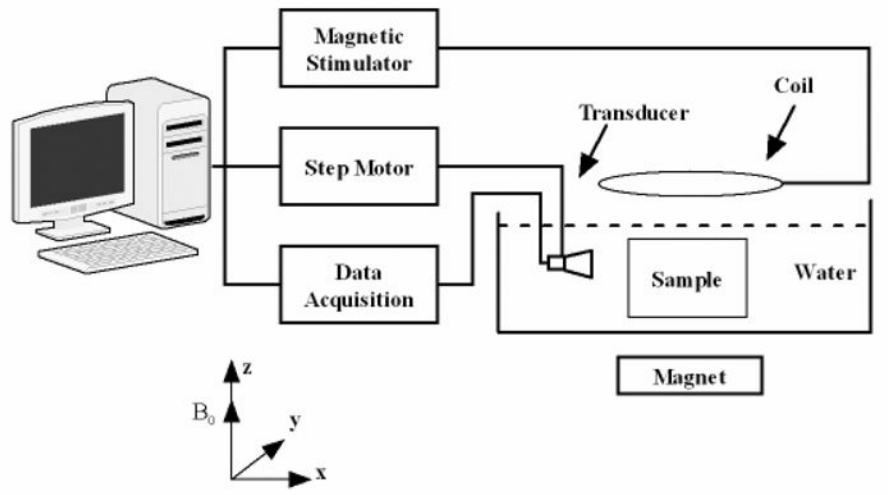

Figure 1.
(Color online) Diagram of the 2-D MAT-MI system setup.

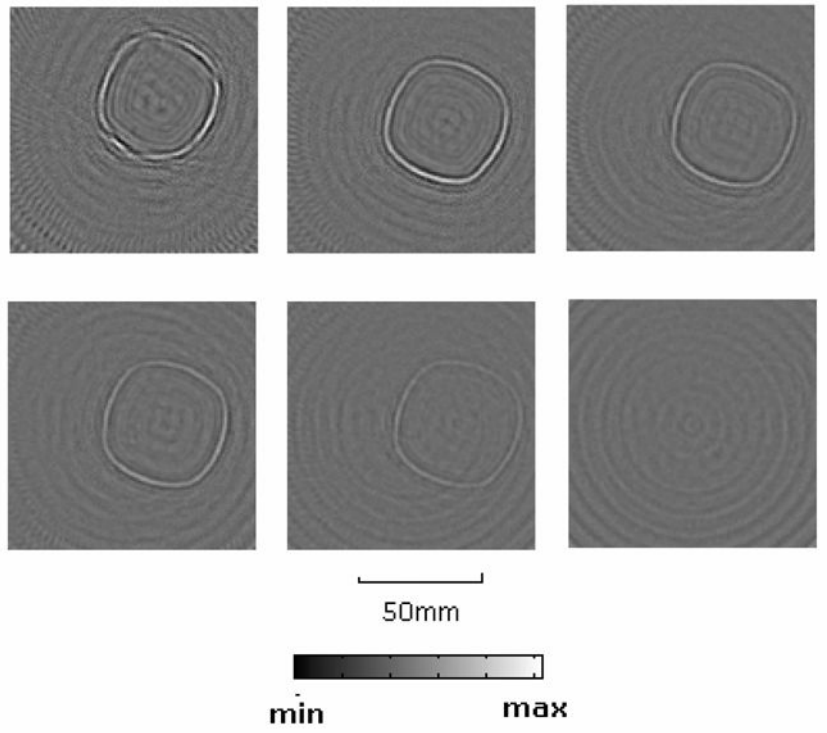

Figure 2.
(Color online) MAT-MI 2-D images of saline samples with different salinities. The salinity is 10%, 8%, 5%, 3%, 1% and 0% from left to right from top to bottom, respectively.

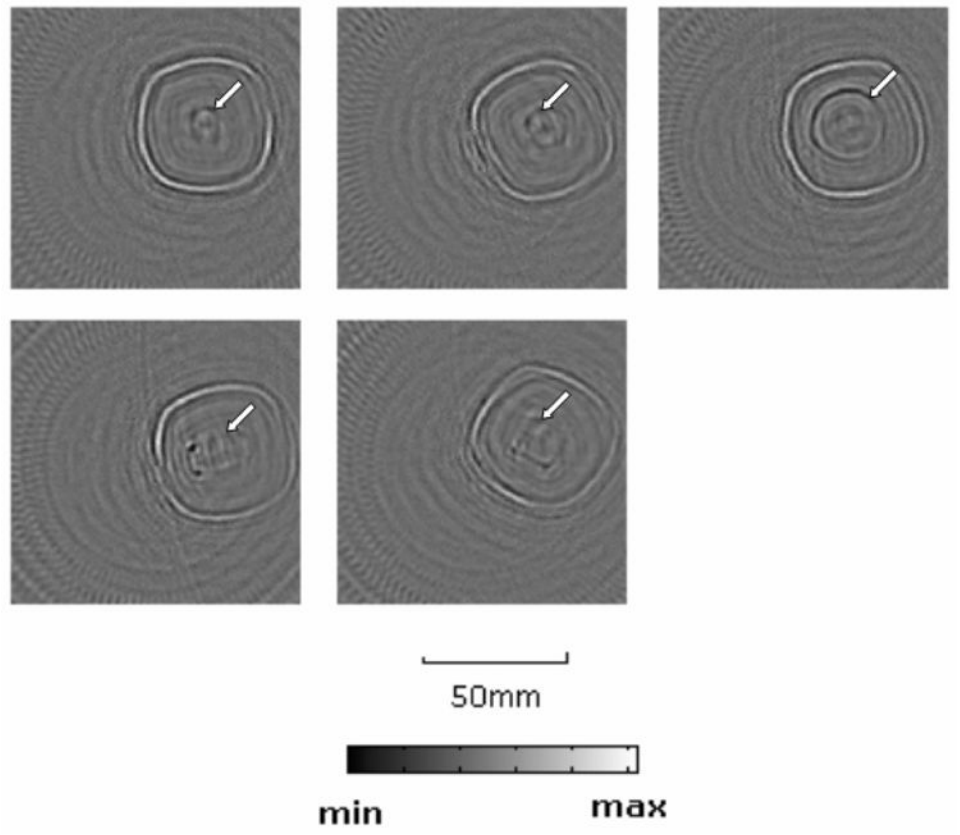

Figure 3.
(Color online) MAT-MI 2-D images of double layer gel phantoms. From top to bottom, left to right, the cross section of the inner layer columns are circles with diameters to be 9mm, 13mm, 26mm, a rectangular with dimension 19mm×10mm and a square with dimension 13mm×13mm, respectively. The reconstructed inner layer conductivity boundaries are marked by red arrows.

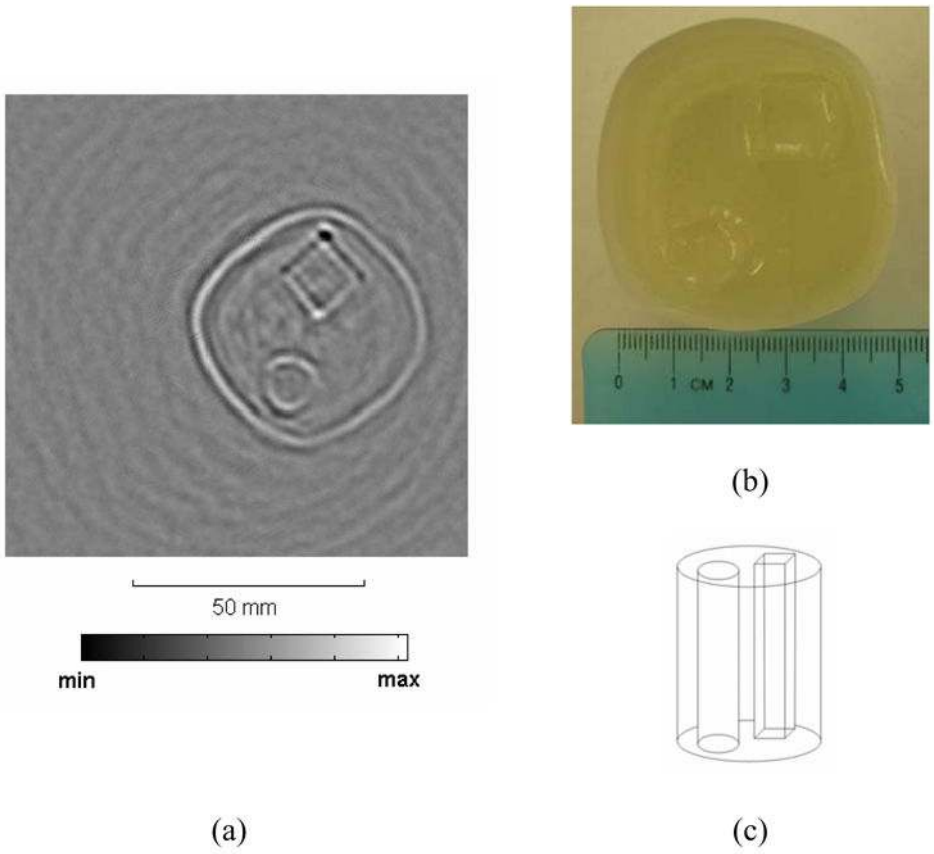

Figure 4.
(Color online) (a) 2-D MAT-MI image of a gel phantom with two columns of gels embedded in. (b) Top view photo of the gel phantom. (c) Diagram of the phantom structure.